AIP | Journal of Applied Physics

Non-destructive characterization of structural hierarchy within aligned carbon nanotube assemblies

Eric Verploegen, A. John Hart, Michael De Volder, Sameh Tawfick, Khek-Khiang Chia et al.

Citation: J. Appl. Phys. **109**, 094316 (2011); doi: 10.1063/1.3584759
View online: http://dx.doi.org/10.1063/1.3584759
View Table of Contents: http://jap.aip.org/resource/1/JAPIAU/v109/i9
Published by the AIP Publishing LLC.

Non-destructive characterization of structural hierarchy within aligned carbon nanotube assemblies

Eric Verploegen,[1,a)] A. John Hart,[2] Michael De Volder,[3] Sameh Tawfick,[2] Khek-Khiang Chia,[4] and Robert E. Cohen[4]
[1]*Department of Materials Science and Engineering, Massachusetts Institute of Technology, 77 Massachusetts Avenue, Cambridge, Massachusetts 02139, USA*
[2]*Mechanosynthesis Group, Department of Mechanical Engineering, University of Michigan, 2350 Hayward Street, Ann Arbor, Michigan, 48109, USA*
[3]*IMEC - KULeuven, Kapeldreef 75, 3001 Heverlee, Belgium*
[4]*Department of Chemical Engineering, Massachusetts Institute of Technology, 77 Massachusetts Avenue, Cambridge, Massachusetts 02139, USA*

(Received 7 December 2010; accepted 25 February 2011; published online 13 May 2011)

Understanding and controlling the hierarchical self-assembly of carbon nanotubes (CNTs) is vital for designing materials such as transparent conductors, chemical sensors, high-performance composites, and microelectronic interconnects. In particular, many applications require high-density CNT assemblies that cannot currently be made directly by low-density CNT growth, and therefore require post-processing by methods such as elastocapillary densification. We characterize the hierarchical structure of pristine and densified vertically aligned multi-wall CNT forests, by combining small-angle and ultra-small-angle x-ray scattering (USAXS) techniques. This enables the nondestructive measurement of both the individual CNT diameter and CNT bundle diameter within CNT forests, which are otherwise quantified only by delicate and often destructive microscopy techniques. Our measurements show that multi-wall CNT forests grown by chemical vapor deposition consist of isolated and bundled CNTs, with an average bundle diameter of 16 nm. After capillary densification of the CNT forest, USAXS reveals bundles with a diameter >4 μm, in addition to the small bundles observed in the as-grown forests. Combining these characterization methods with new CNT processing methods could enable the engineering of macro-scale CNT assemblies that exhibit significantly improved bulk properties. © *2011 American Institute of Physics*. [doi:10.1063/1.3584759]

I. INTRODUCTION

Carbon nanotubes (CNTs) have attracted significant interest due to their remarkable mechanical, electrical, and thermal properties.[1–3] Many applications require assemblies of CNTs rather than individual CNTs, and therefore insight into the formation and structure of CNT assemblies is important. In organic electronics such as field effect transistors,[4,5] chemical sensors,[6,7] interconnects,[8,9] and transparent electrodes,[10,11] the contact between the individual CNTs within thin films determines the charge transfer characteristics. Therefore, CNT films with a maximized number of contacts to ensure a percolation path for charge transport are needed.[9,12] The control of CNT bundling and debundling is important for the dispersion of CNTs in solvents and matrix materials (e.g., polymers), and controlling interactions between CNTs and matrix materials is vital for creating CNT-polymer composite materials having high strength and attractive multifunctional properties.[13–18] Furthermore, the mechanical and electrical properties of CNT yarns[19,20] which could eventually surpass graphite fibers, are affected by the internal arrangement of the CNTs including the alignment, bundle size, and the possible presence of voids.[21] Therefore, in order to engineer the properties of CNT materials for these applications it is critical to understand and control the hierarchical morphology of CNTs within assemblies. We demonstrate the utility of ultra-small-angle x-ray scattering (USAXS) for nondestructively characterizing hierarchical multi-wall CNT ensembles grown by chemical vapor deposition (CVD).[22]

Specifically, we use USAXS to characterize vertically aligned CNTs, also known as "CNT forests." In forest growth, the CNTs self-align due to crowding at the initial stage of growth,[23] forming an anisotropic structure that seeks to utilize the attractive axial properties of a large number of CNTs (typically $> 10^{10}$ CNTs/cm^2) in parallel. Although this process is well established, the CNT density per area is low, and therefore the bulk properties of CNT forests are far below those of individual CNTs. The density of a typical CNT forest is 10^{11}–10^{12} CNTs per square centimeter (assuming $\approx$10 nm diameter), whereas forest densities higher than 10^{13} CNTs per square centimeter are needed to match the electrical conductivity of copper.[24] Therefore, two main approaches have been developed to increase the CNT density after growth. The first method consists of mechanically densifying the CNTs by applying compressive forces.[25,26] In the second method the CNT forests are submerged in a solvent that wets the CNTs, causing elastocapillary aggregation due to surface tension between the CNTs and the liquid.[20,23,27–34] Here, we investigate the hierarchical structure of CNT forests in their

a)Author to whom correspondence should be addressed. Electronic mail: ericverp@stanford.edu.

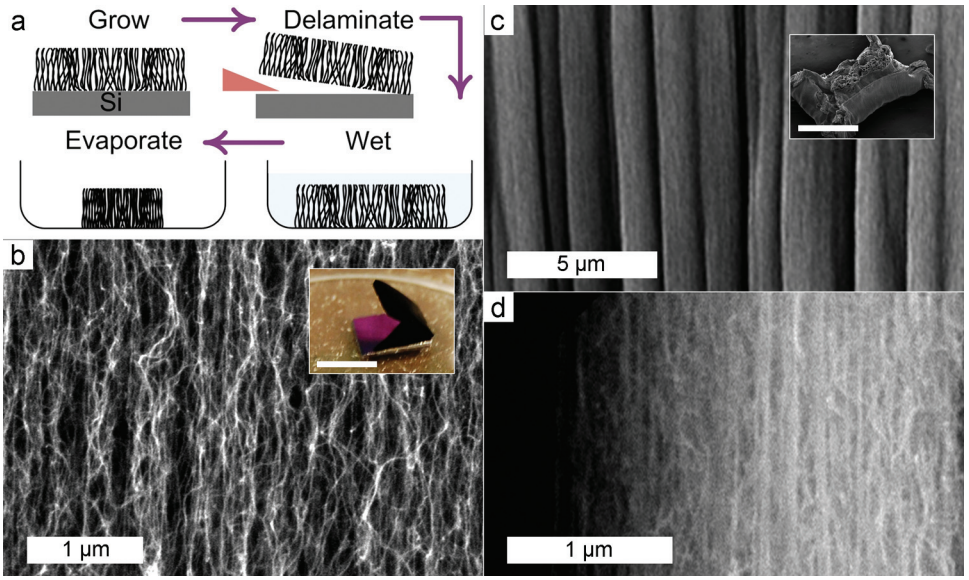

FIG. 1. (Color online) (a) Diagram of the CNT forest densification process; (b) SEM image showing the alignment within the sidewall of the pristine CNT forest after growth, with inset photograph showing the delaminated forest on the silicon substrate (scale: 5 mm); (c) Densified morphology of the CNT forest sidewall after wetting and evaporation of ethanol, with inset SEM image showing the entire densified forest (scale: 1 mm); (d) Close up SEM image of the densified morphology, showing the high density and alignment of the individual bundle.

pristine as-grown state, and after capillary densification using an organic solvent.

II. METHODS

Multi-wall CNT forests are grown by atmospheric pressure thermal CVD, using a catalyst film of Fe/Al_2O_3 deposited on a silicon wafer.[22] The investigated CNT forests cover an area of ~ 0.5 cm^2, are 0.5 mm tall, and can easily be delaminated from the substrate by gently lifting one edge of the forest with a razor blade. As illustrated in Fig. 1, elastocapillary densification was achieved by wetting a free-standing CNT forest with ethanol and letting evaporation occur at ambient conditions, due to the fact that as the solvent evaporates, the CNTs are pulled closer together. Due to the highly oriented nature of the CNT forest, the densification is essentially planar, as shown in Fig. 1. However, as the forest contracts laterally, the edges of the forest wrinkle and fold as shown in Fig. 1(c). The forests investigated in this study displayed areal densification (reduction in the area of the forest in the plane of the substrate) of 87%. However, due to the presence of microscopic voids in the densified forest, the densification is locally greater. In forests with smaller initial lateral dimensions, densification up to 95% was observed, representing a 20-fold increase over the pristine state.

We previously used small angle x-ray scattering (SAXS) to nondestructively measure the average diameter and the orientation of the CNTs as a function of position within vertically aligned forests,[35,36] and to develop collective models of growth kinetics;[53,54] however conventional SAXS techniques typically cannot probe the q range below 0.1 nm^{-1}.[37] USAXS can probe $q = 0.001$–0.4 nm^{-1}, enabling features larger than one micron to be resolved.[38–41] Thus, SAXS and USAXS can be used in a complementary fashion to access the q range that includes the form factor scattering from isolated CNTs, the structure factor scattering between neighboring tubes, and the Debye-Büche scattering from the CNT bundles. The scattering intensity, I, as a function of scattering angle, q, can be described by Eq. (1), where A is an adjustable constant that accounts for instrumental and other experimental factors, $F(q)$ is the form factor, $S(q)$ is the structure factor, and $C(q)$ is the Debye-Büche function,

$$I(q) = AF(q)S(q) + C(q). \tag{1}$$

The form factor, $F(q)$, describes the scattering from the cross section of isolated tubes. We use a core-shell cylinder form factor model[42,43] to represent the individual CNTs, where R is the geometric radius of the CNT, c is ratio of inner radius to the outer radius, J_1 is a Bessel function of the first kind, and $P(R)$ is a function that provides a Gaussian distribution of the CNT radii,

$$F(q) = \frac{1}{q}\left[\frac{2J_1(qR) - cJ_1(cqR)}{qR(1-c^2)}\right]^2. \tag{2}$$

The structure factor, $S(q)$, describes the scattering between neighboring CNTs. Oster and Riley[44] developed an expression for the structure factor for cylinders aligned perpendicular to the SAXS beam with arbitrary distances between neighbors, where v is the in-plane number density of cylinders, s is the separation between cylinder centers, and J_1 is a Bessel function of the first kind,

$$S(q) = 1 - \upsilon\pi S^2\left[\frac{2J_1(qs)}{qs}\right]. \tag{3}$$

The second term, $C(q)$, is the Debye-Büche function,[37,45] which we use to describe the contribution from the CNT bundles, where I_o is a constant related to the average mass and ζ is the characteristic bundle size,

$$C(q) = \frac{I_o}{\left(1+q^2\zeta^2\right)^2}. \tag{4}$$

The USAXS experiments were conducted at XOR sector 32-ID at the Advanced Photon Source, Argonne National

Laboratory. The USAXS instrument employs a side-bounce Bonse–Hart-type geometry in an undulator beamline.[41] The CNT forest was oriented relative to the analyzer crystals such that only scattering perpendicular to the growth direction was measured; hence, providing information about the morphology in the direction of the densification. The commercially available software Igor Pro, from WaveMetrics Inc., was used for processing the raw data. A reduction of the raw instrument data and desmearing was performed using the macros Indra and Irena, respectively, which were developed by Jan Ilavsky (Argonne National Laboratory, http://usaxs.xor.aps.anl.gov) for use with Igor Pro.

III. RESULTS AND DISCUSSION

We used small-angle x-ray scattering (SAXS), at the Cornell High Energy Synchrotron Source (CHESS), to probe the higher q regime, $0.2\ \text{nm}^{-1} < q < 1.6\ \text{nm}^{-1}$. Using the previously described formalism[35,36] we found the CNTs within the forest have an average outer diameter of 11.2 ± 2.4 nm, with a ratio of the inner diameter to outer diameter of 0.62 (details provided in the supplementary material[46]). These values were then used in the form factor component of the model for the USAXS data, which provides the data from the lower q range, $0.001\ \text{nm}^{-1} < q < 0.4\ \text{nm}^{-1}$. The USAXS data for the pristine and densified forests are shown in Fig. 2, along with the results of numerical optimization of the models.

In the pristine forest the dominant contribution to the scattering is from the Debye-Büche term, $C(q)$, resulting in the shoulder observed near $3 \times 10^{-2}\ \text{nm}^{-1}$, indicating a bundle size of 16.2 ± 1.4 nm. The diameter of 16.2 nm indicates that there are a significant number of CNTs that are paired with another CNT through Van der Waals attractions, forming what is essentially a bundle of two or three CNTs. Due to the tortuosity [see Fig. 1(b)] and the high aspect ratio of the CNTs we do not expect that the same CNTs are in contact over the entire length of the forest; rather, some portions of CNTs come in contact with one another, and the rest of the CNT does not interact with other CNTs. The tortuosity observed in the SEM also indicated that a given CNT may come in contact with many different other CNTs over the length of the forest; these interactions enable the CNTs to organize into a forest during growth. The Guinier regime, which is the flat region observed at $q < 2 \times 10^{-2}\ \text{nm}^{-1}$, indicates that there are few, if any, bundles larger than 16.2 nm that significantly contribute to the scattering. Figure S2 in the supplementary material[46] describes the contributions from each term to the USAXS profile.

For the densified forest, two independent Debye-Büche function terms were used to describe the hierarchically structured CNT bundles. The first Debye-Büche term, $C_1(q)$, describes the smaller features with a diameter of 12.6 ± 0.85 nm. This feature size is essentially the same as the individual tube diameter, 11.2 ± 2.4 nm; thus, these "bundles" represent individual tubes. The second Debye-Büche term, $C_2(q)$, accounts for the $I(q)$ versus q slope of 10^{-4} at $q < 10^{-2}\ \text{nm}^{-1}$, indicating that there are bundles larger than 4 μm. We can only give a lower bound on the bundle size due to the resolution limit of the instrument at very low q. These results do not exclude the possibility of bundles between 12 nm and 4 μm; it is most likely that there is a distribution of bundle sizes across this size range, which would not significantly contribute to the scattering. The change in the slope of the low q scattering from 0 to 10^{-4} clearly indicates the formation of these larger CNT bundles upon capillary densification.

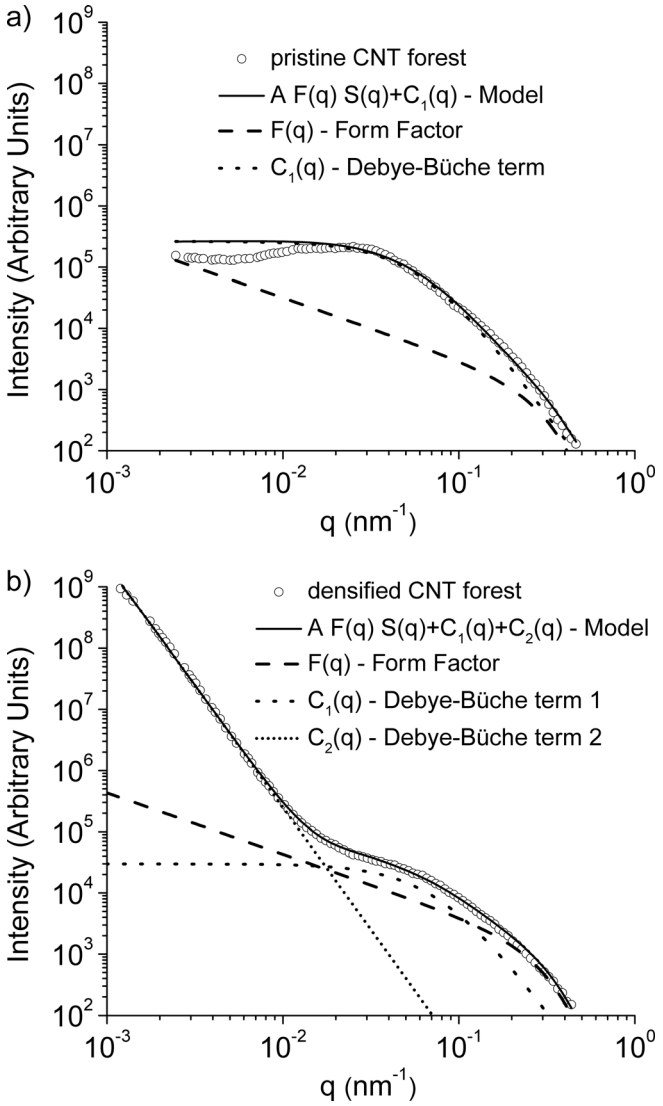

FIG. 2. Desmeared USAXS data of (a) pristine CNT forest and (b) densified CNT forest. The model fit for each data set is shown with a solid line. The contributions from all terms to the total model fit are shown in the supplementary material (Ref. 46).

We correlate these findings to calculations of bundle sizes based on a model of elastocapillary aggregation. As described in previous studies, capillary forces tend to aggregate fibers into foamy structures. This phenomenon has been studied for the aggregation of wet hair,[47] nano- and microfibers,[48,49] micropillars,[50] and CNTs.[23,27,34,51,52] We base our analysis on a model described by Py *et al.*[48] Even though the forest is delaminated from the substrate before densification, it is still constrained on the top surface due to the "crust" layer of entangled CNTs that forms at the start of growth.[23,35,36] We model the CNTs as an arrangement of

FIG. 3. (Color online) One-dimensional schematic of CNT self-assembly due to elastocapillary aggregation.

initially parallel beams, which does not account for the tortuosity of the CNTs within the forest.

During elastocapillary aggregation, surface tension pairs the CNTs in a hierarchical fashion, starting from the constraint surface (crust) as shown schematically in Fig. 3. At a certain distance, L_I, from the crust, two CNTs will be joined together. The distance, L_I, is determined by the equilibrium between surface tension forces and elastic restoring forces. This pair of CNTs will aggregate with another pair of CNTs at a distance, L_S, from the substrate, forming a bundle. This process proceeds until complex micrometer-sized bundles are formed.

Following Py *et al.*,[48] L_I is defined as

$$L_I = \left[\frac{9}{2(\pi-2)}\right]^{1/4}\sqrt{d\sqrt{\frac{E\pi R^3}{4\gamma}}}, \tag{5}$$

where d is the spacing between adjacent CNTs, E is the Young's modulus (1 TPa), R is the CNT radius (5.6 nm), and γ is the surface tension (0.025 N/m for ethanol). The spacing is taken as the average spacing within the forest, which, based on density measurements, is calculated to be approximately 100 nm. For these model parameters L_I is approximately 700 nm. Finally, at a given distance from the substrate, L_S, successive pairing of CNTs bundles forms a hierarchical structure

$$L_S = L_I\left[\frac{\beta^2(\pi-2)}{2\sqrt{\pi}3^{1/4}(2-\sqrt{2})}\right]^{1/4}N^{3/8}. \tag{6}$$

Here, N is the number of individual CNTs in the bundle and β accounts for the lattice geometry and the sticking scenario, which is set equal to 0.5 based on previous experiments.[34]

Figure 4 shows the diameter of the densified bundles as a function of L_S. This graph shows that 4 μm bundles are expected to be present about 30 μm from the constraint surface. Between 30 and 100 μm from the constraint surface, we expect to have bundles with a diameter between 4 and 20 μm. In other words, for forests with a height of a few hundred micrometers as tested in these experiments, the above model confirms that most of the CNTs should form bundles with a diameter of more than 4 μm, as confirmed experimentally in the USAXS measurements. Practically, the crust layer is not a perfect constraint; rather it consists of a sheet of highly entwined CNTs that can be compressed to a certain extent by surface tension. In our calculations, we assumed the crust to be perfectly rigid, so in practice the predominant bundle size should be even larger than calculated. Full aggregation into a uniformly dense bundle is prevented due to the entwined nature of the crust layer. A SEM image showing the top of the CNT forest can be found in Fig. S1 of the supplementary material.[46]

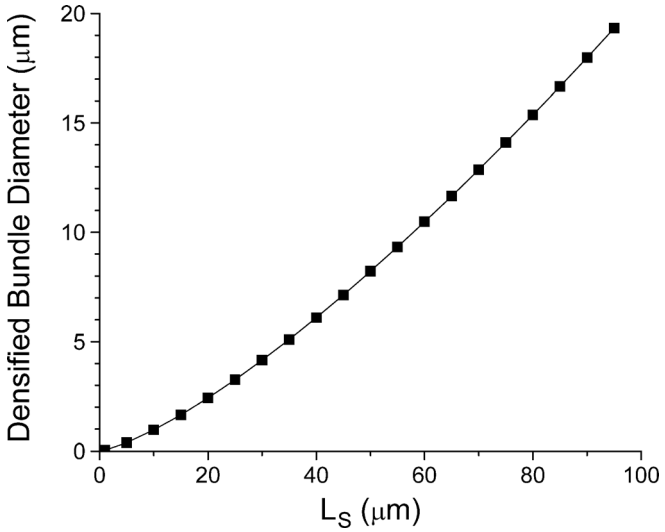

FIG. 4. The densified CNT bundle diameter as a function of L_S, computed from Eqs. (5) and (6). Details on the calculation of the CNT bundle diameter can be found in the supplementary material (Ref. 46).

IV. CONCLUSION

We have demonstrated that SAXS and USAXS can be combined to nondestructively measure the diameter and bundle size of CNTs within assemblies, spanning length scales from nanometers to micrometers. These techniques revealed that elastocapillary densification of CNTs caused the assembly of bundles exceeding 4 μm in diameter, compared to bundles of 16 nm in pristine forests. We corroborated these measurements with a model of elastocapillary aggregation, which accounts for the top crust on the forest that prevents complete densification.

Combining the characterization techniques presented here with improvements in CNT processing techniques can assist the engineering of CNT assemblies such as films, yarns, and composite materials with novel multifunctional properties.

ACKNOWLEDGMENTS

Research at the APS is supported by the U.S. Department of Energy, Office of Science, Basic Energy Sciences under Contract No. W-31-109-Eng-38. CHESS is supported by the NSF & NIH/NIGMS via NSF Grant No. DMR-0225180. This work was sponsored by the U.S. Army Research Office through the Institute for Soldier Nanotechnologies at MIT under Contract No. DAAD-19-02-D0002; by the National Science Foundation (Grant No. CMMI-0800213); and by the University of Michigan Department of Mechanical Engineering and College of Engineering. E.V. thanks the Eastman Kodak Corporation and the Kodak Fellows Program for support. M. D. V. thanks the Fund for Scientific Research–Flanders, Belgium. K.K.C. thanks the

MRSEC Program of the National Science Foundation under Grant No. DMR-02-13282 for support. We thank Jan Ilavsky for help with the USAXS measurements and data analysis.

[1]R. H. Baughman, A. A. Zakhidov, and W. A. de Heer, Science **297**, 787 (2002).
[2]M. S. Dresselhaus, G. Dresselhaus, and P. C. Eklund, *Science of Fullerenes and Carbon Nanotubes* (Academic, San Diego, 1996).
[3]H. W. Zhu and B. Q. Wei, J. Mater. Sci.Technol. **24**, 447 (2008).
[4]M. C. LeMieux, M. Roberts, S. Barman, Y. W. Jin, J. M. Kim, and Z. N. Bao, Science **321**, 101 (2008).
[5]R. Seidel, A. P. Graham, E. Unger, G. S. Duesberg, M. Liebau, W. Steinhoegl, F. Kreupl, and W. Hoenlein, Nano Lett. **4**, 831 (2004).
[6]F. Wang, H. W. Gu, and T. M. Swager, J. Am. Chem. Soc. **130**, 5392 (2008).
[7]K. Besteman, J. O. Lee, F. G. M. Wiertz, H. A. Heering, and C. Dekker, Nano Lett. **3**, 727 (2003).
[8]N. Chiodarelli, K. Kellens, D. J. Cott, N. Peys, K. Arstila, M. Heyns, S. De Gendt, G. Groeseneken, and P. M. Vereecken, J. Electrochem. Soc. **157**, K211 (2010).
[9]P. Avouris, Z. H. Chen, and V. Perebeinos, Nat. Nanotechnol. **2**, 605 (2007).
[10]H. Gu and T. M. Swager, Adv. Mater. **20**, 4433 (2008).
[11]J. van de Lagemaat, T. M. Barnes, G. Rumbles, S. E. Shaheen, T. J. Coutts, C. Weeks, I. Levitsky, J. Peltola, and P. Glatkowski, Appl. Phys. Lett. **88**, 233503 (2006).
[12]P. Sharma and P. Ahuja, Mater. Res. Bull. **43**, 2517 (2008).
[13]J. Njuguna, K. Pielichowski, and J. R. Alcock, Adv. Eng. Mater. **9**, 835 (2007).
[14]B. L. Wardle, D. S. Saito, E. J. Garcia, A. J. Hart, R. G. de Villoria, and E. A. Verploegen, Adv. Mater. **20**, 2707 (2008).
[15]P. M. Ajayan and J. M. Tour, Nature (London) **447**, 1066 (2007).
[16]R. Andrews, D. Jacques, A. M. Rao, T. Rantell, F. Derbyshire, Y. Chen, J. Chen, and R. C. Haddon, Appl. Phys. Lett.**75**, 1329 (1999).
[17]A. B. Dalton, S. Collins, E. Munoz, J. M. Razal, V. H. Ebron, J. P. Ferraris, J. N. Coleman, B. G. Kim, and R. H. Baughman, Nature (London) **423**, 703 (2003).
[18]B. Vigolo, A. Penicaud, C. Coulon, C. Sauder, R. Pailler, C. Journet, P. Bernier, and P. Poulin, Science **290**, 1331 (2000).
[19]K. Koziol, J. Vilatela, A. Moisala, M. Motta, P. Cunniff, M. Sennett, and A. Windle, Science **318**, 1892 (2007).
[20]J. G. Fan, D. Dyer, G. Zhang, and Y. P. Zhao, Nano Lett. **4**, 2133 (2004).
[21]S. L. Fang, M. Zhang, A. A. Zakhidov, and R. H. Baughman, J. Phys.: Condens. Matter **22**, 334221 (2010).
[22]A. J. Hart and A. H. Slocum, J. Phys. Chem. B **110**, 8250 (2006).
[23]M. F. L. De Volder, D. O. Vidaud, E. R. Meshot, S. Tawfick, and A. J. Hart, Microelectron. Eng. **87**, 1233 (2010).
[24]A. Romo-Negreira, O. Richard, S. D. Gendt, K. Maex, M. M. Heyns, and P. M. Vereecken, Sci. Technol. Adv. Mater. **1**, 86 (2009).
[25]C. L. Pint, Y. Q. Xu, M. Pasquali, and R. H. Hauge, ACS Nano **2**, 1871 (2008).
[26]S. Tawfick, K. O'Brien, and A. J. Hart, Small **5**, 2467 (2009).
[27]N. Chakrapani, B. Q. Wei, A. Carrillo, P. M. Ajayan, and R. S. Kane, Proc. Natl. Acad. Sci. U.S.A. **101**, 4009 (2004).
[28]M. A. Correa-Duarte, N. Wagner, J. Rojas-Chapana, C. Morsczeck, M. Thie, and M. Giersig, Nano Lett. **4**, 2233 (2004).
[29]D. N. Futaba, K. Hata, T. Yamada, T. Hiraoka, Y. Hayamizu, Y. Kakudate, O. Tanaike, H. Hatori, M. Yumura, and S. Iijima, Nature Mater. **5**, 987 (2006).
[30]Y. Hayamizu, T. Yamada, K. Mizuno, R. C. Davis, D. N. Futaba, M. Yumura, and K. Hata, Nature Nanotechnol. **3**, 289 (2008).
[31]K. K. S. Lau, J. Bico, K. B. K. Teo, M. Chhowalla, G. A. J. Amaratunga, W. I. Milne, G. H. McKinley, and K. K. Gleason, Nano Lett. **3**, 1701 (2003).
[32]H. Liu, S. H. Li, J. Zhai, H. J. Li, Q. S. Zheng, L. Jiang, and D. B. Zhu, Angew. Chem., Int. Ed. **43**, 1146 (2004).
[33]Z. Liu, N. Bajwa, L. Ci, S. H. Lee, S. Kar, P. M. Ajayan, and J.-Q. Lu, *International Interconnect Technology Conference* (IEEE, New York, 2007), p. 201.
[34]M. De Volder, S. H. Tawfick, S. J. Park, D. Copic, Z. Zhao, W. Lu, and A. J. Hart, Adv. Mater. **22**, 4384 (2010).
[35]B. N. Wang, R. D. Bennett, E. Verploegen, A. J. Hart, and R. E. Cohen, J. Phys. Chem. C **111**, 17933 (2007).
[36]B. N. Wang, R. D. Bennett, E. Verploegen, A. J. Hart, and R. E. Cohen, J. Phys. Chem. C **111**, 5859 (2007).
[37]H. Brumberger, *Modern Aspects of Small-Angle Scattering* (Kluwer Academic, Dordrecht, Boston, 1995).
[38]L. E. Levine and G. G. Long, Journal of Applied Crystallography **37**, 757 (2004).
[39]F. Zhang, G. G. Long, L. E. Levine, J. Ilavsky, and P. R. Jemian, J. Appl. Crystallogr. **41**, 416 (2008).
[40]F. Zhang and J. Ilavsky, Polym. Rev. **50**, 59 (2010).
[41]J. Ilavsky, P. R. Jemian, A. J. Allen, F. Zhang, L. E. Levine, and G. G. Long, J. Appl. Crystallogr. **42**, 469 (2009).
[42]T. Inada, H. Masunaga, S. Kawasaki, M. Yamada, K. Kobori, and K. Sakurai, Chem. Lett. **34**, 524 (2005).
[43]K. Lu, J. Jacob, P. Thiyagarajan, V. P. Conticello, and D. G. Lynn, J. Am. Chem. Soc. **125**, 6391 (2003).
[44]G. Oster and D. P. Riley, Acta Crystallogr. **5**, 272 (1952).
[45]D. Pontoni and T. Narayanan, J. Appl. Crystallogr. **36**, 787 (2003).
[46]See supplementary material at http://dx.doi.org/10.1063/1.3584759 for additional SEM images, details of the models used for fitting USAXS data, and details of the elastocapillary aggregation model.
[47]J. Bico, B. Roman, L. Moulin, and A. Boudaoud, Nature (London) **432**, 690 (2004).
[48]C. Py, R. Bastien, J. Bico, B. Roman, and A. Boudaoud, Europhys. Lett. **77**, 44005 (2007).
[49]B. Pokroy, S. H. Kang, L. Mahadevan, and J. Aizenberg, Science **323**, 237 (2009).
[50]H. Namatsu, K. Kurihara, M. Nagase, K. Iwadate, and K. Murase, Appl. Phys. Lett. **66**, 2655-2657 (1995).
[51]C. Journet, S. Moulinet, C. Ybert, S. T. Purcell, and L. Bocquet, Europhys. Lett. **71**, 104 (2005).
[52]Y. P. Zhao and J. G. Fan, Appl. Phys. Lett. **88**, 103123 (2006).
[53]E. R. Meshot, M. Bedewy, K. M. Lyons, A. R. Woll, K. A. Juggernauth, S. Tawfick, and A. J. Hart, Nanoscale **2**, 896 (2010).
[54]M. Bedewy, E. R. Meshot, H. C. Guo, E. A. Verploegen, W. Lu, and A. J. Hart, J. Phys Chem. C, **113**, 20576 (2009).